Science Advances

AAAS

advances.sciencemag.org/cgi/content/full/3/6/e1602569/DC1

Supplementary Materials for

Wind-invariant saltation heights imply linear scaling of aeolian saltation flux with shear stress

Raleigh L. Martin and Jasper F. Kok

Published 7 June 2017, *Sci. Adv.* **3**, e1602569 (2017)
DOI: 10.1126/sciadv.1602569

The PDF file includes:

Other Supplementary Material for this manuscript includes the following:
(available at advances.sciencemag.org/cgi/content/full/3/6/e1602569/DC1)

- data file S1 (Microsoft Excel format). Excel spreadsheet (.xlsx) containing unbinned 30-min values for shear velocity u_*, shear stress τ, wind direction θ, stability parameter z/L, saltation layer height z_q, total saltation flux Q, saltation detection frequency f_Q, and associated uncertainties for all of these values (except θ, z/L, and f_Q) for each field site.
- data file S2 (Microsoft Excel format). Excel spreadsheet (.xlsx) containing binned 30-min values for shear velocity u_*, shear stress τ, excess shear stress τ_{ex}, saltation

layer height z_q, total saltation flux Q, normalized saltation flux $\hat{Q}$, saltation detection frequency f_Q, and associated uncertainties for all of these values.

Supplementary Materials

Overview

In this supplementary document, we present detailed descriptions of wind and saltation calculations, data binning procedures, sources of literature data, and data fitting. This document elaborates on descriptions of field sites, instrumentation, and saltation flux calibration described in *(83)*. We conclude with a detailed list of all variables used in the main text and supplementary text, six supplementary figures, and descriptions of two supplementary data sets.

Calculation of physical values from wind and saltation data

In this section, we describe methods for processing raw measurements into meaningful physical variables describing the properties of the wind and saltation layer over successive 30-minute analysis time intervals. Further detailed descriptions of field sites, instrumentation, and calibration of saltation fluxes are provided in *(83)*.

Generation of 30-minute analysis intervals

We performed all wind and saltation calculations over 30-minute time intervals. As in Kok et al. *(84)*, we chose 30 minutes as sufficiently long to integrate over the longest period of turbulent fluctuations but short enough to resolve meteorological variations driving fluctuations in saltation flux *(56)*. In particular, we considered successive 30-minute windows for which sonic anemometer, Wenglor, and BSNE sand trap data were available and spanned the whole time window. This requirement for BSNE data was set to ensure accuracy of the flux calibration. In our analyses, we also included data from time intervals in which Wenglor data were not collected but saltation flux was known to be zero. These additional time intervals provide bases for comparison of wind properties during non-saltation intervals.

Wind data processing

In this subsection, we describe our wind data processing methodology. This includes selection of anemometers, reorientation of wind velocity vectors to align with the direction of mean wind, diagnostic calculations of the wind direction and stability parameter, and computation of wind shear stress and shear velocity. Most of our methods follow standard practices for wind data processing.

Although we deployed sonic anemometers at multiple heights *(83)*, we utilized observations only from the lowest sonic anemometer at each site for the analyses described in this paper. These lowermost anemometers were positioned about half a meter above the ground surface. We selected the lowest anemometers as most representative of shear stress at the bed and least likely to be affected by boundary layer instability farther from the surface. To be sure that our results were not biased by choice of anemometer, we compared all of our analyses to those generated by using the second highest anemometer in the profile. We found no significant differences in the outcome of our analyses if using the lowest versus the second lowest anemometer in the profile.

Although we mounted sonic anemometers to align with the mean streamwise wind, instrument alignment in practice was imperfect and wind direction varied through time. The variation in wind direction can be described by wind angles θ, calculated as

$$\theta = \tan^{-1}\left(\frac{\bar{v}}{\bar{u}}\right) - \langle\theta\rangle \qquad \text{(S1)}$$

where $\bar{u}$ and $\bar{v}$ are respectively the raw mean streamwise and spanwise wind over a 30-minute interval, and $\langle\theta\rangle$ is the site-averaged wind angle during saltation. θ therefore describes the deviation of the wind direction during a given 30-minute interval from the typical wind during saltation. Figure S1 shows wind angles during 30-minute intervals compared to shear velocities u_* for those same intervals. Separate symbols are used to denote 30-minute intervals with and without detected saltation. Although some of the wind angles in the figure diverge substantially from the mean, this variation is limited to a range of $\theta = \pm 20°$ during periods of saltation, indicating the occurrence of one predominant wind direction during each of the three deployments.

Following standard practice, we applied a streamline correction *(56)* to reorient wind velocities, such that $\bar{v} = \bar{w} = 0$ over each 30-minute calculation time interval. Thus, for these intervals, the streamline-corrected mean streamwise wind was $\bar{u} = \langle\sqrt{u^2 + v^2 + w^2}\rangle$, where the angle brackets $\langle\ \rangle$ denote the average over all instantaneous wind vectors. We then calculated shear stresses τ by the Reynolds stress method (equation 17) applied to the streamline-corrected winds. We calculated uncertainty in 30-minute shear stress σ_τ using the script "random_error.m" provided as a supplement to Salesky et al. *(87)*. We used the Reynolds stress method instead of the law-of-the-wall for stress calculations, because the latter is potentially subject to bias from changes in the von Karman parameter *(88)* or other modifications of the near-surface wind velocity profile by the effects of saltation *(89)*.

We calculated wind shear velocity from wind shear stress by equation 3 (main text), and we calculated the associated shear velocity uncertainty as

$$\sigma_{u_*} = \frac{\sigma_\tau}{2\rho_f u_*} \tag{S2}$$

To obtain equation S2, we applied the error propagation equation for uncorrelated variables *(equation 3.14 in 90)*

$$\sigma_y = \sqrt{\sigma_{x_1}^2 \left(\frac{\partial y}{\partial x_1}\right)^2 + \sigma_{x_2}^2 \left(\frac{\partial y}{\partial x_2}\right)^2 + \cdots} \tag{S3}$$

where the variable y is a function of the quantities x_1, x_2, ... with uncorrelated uncertainties $\sigma_{x_1}, \sigma_{x_2}, \ldots$.

As a diagnostic for the quality of shear stress estimates, we computed the stability parameter z/L for all 30-minute intervals. $z/L \approx 0$ indicates neutrally stable conditions, in which mechanical production of turbulence is dominant and buoyant production is negligible. We computed the stability parameter as

$$\frac{z}{L} = \frac{-(g/T)\langle T'w'\rangle}{u_*^3/\kappa z_U} \tag{S4}$$

where g is gravitational acceleration ($= 9.8$ m s^{-2}), T is air temperature (K), T' is the fluctuating component of temperature ($T' = T - \bar{T}$, where $\bar{T}$ is mean temperature), κ is the von Karman parameter ($\approx$0.4), and z_U is anemometer height.

Values of $\frac{z}{L}$ are shown in fig. S2. In most cases, $\frac{z}{L} < 0$, indicating slightly to moderately unstable daytime conditions. During time intervals when saltation transport is detected, $\left|\frac{z}{L}\right| < 0.15$, indicating that the degree of instability is small *(87)* and conditions are close to neutral stability near the surface where saltation is measured.

Saltation flux data processing

Our methods for determining 30-minute saltation layer heights and fluxes are the subject of extensive new methodological development described in *(83)*. We briefly summarize this methodology here. Our saltation calculations combined measurements from BSNE sand traps and Wenglor optical particle counters. The BNSEs provided reliable absolute measures of saltation flux but with poor time resolution (~1/hr). The Wenglors offered excellent time resolution (25 Hz), but their particle counts provided only a relative measure of the saltation flux. Therefore, we used BSNE trap measurements to calibrate the Wenglor particle counts into physically meaningful flux values. Then, we subsampled the calibrated Wenglor fluxes at our desired 30-minute intervals to obtain vertical profiles of horizontal saltation flux $q(z)$, from which we calculated saltation heights z_q by fitting to equation 4 (main text) and total saltation fluxes Q by equation 11 (main text). An example of a 30-minute saltation flux profile $q(z)$ with associated uncertainties is shown in fig. S3. The exponential nature of such a profile is clearly apparent in the decay of the saltation flux profile q with height of the Wenglor z.

Comparison of 30-minute saltation and wind values

30-minute saltation layer heights z_q are compared to shear velocities u_* in fig. S4, and corresponding total saltation fluxes Q are compared to shear stresses τ in fig. S5. These plots qualitatively support the main findings of our study – that z_q does not vary with u_*, and that Q

increases linearly with τ above a minimum threshold value. However, these plots also display variability among 30-minute values that is substantially larger than the random errors denoted by individual error bars, indicating the presence of unexplained systematic uncertainty in the saltation-wind relationship. Such systematic uncertainty could be driven by variability in large-scale turbulence structures *(46)* or soil characteristics *(47)*, factors that we expect to investigate in future studies. To account for such systematic uncertainty in saltation and wind measurements without explicitly determining its origins, we grouped individual 30-minute values into bins as described below.

Data binning and uncertainty estimation

In this section, we describe our procedures for aggregating calculations from individual 30-minute time intervals into bins covering ranges of shear stress τ for each field site. By sorting data into bins, we were able to obtain statistically representative values for saltation height z_q and total saltation flux Q and to quantify the associated systematic uncertainties for these values. Binning also provided an objective basis for conditioning analyses on specific ranges of transport frequency. We henceforth apply 'i' subscripts to distinguish binned values from individual 30-minute values without subscripts.

Creation of shear stress bins

For each site, we categorized each 30-minute value into a bin based on the 30-minute shear stress τ during the associated time interval. Therefore, each bin *i* was defined by a range of shear stresses, $[\tau_{min,i}, \tau_{max,i}]$. Ideally, such bins would have been uniformly constructed such that $\tau_{max,i} - \tau_{min,i}$ was the same for all bins. However, due to natural fluctuations in the wind, the τ were not equally spaced across the full range of possible shear stresses at each site. To balance the priorities of including sufficient data points in each bin while avoiding creation of bins spanning excessively wide ranges of τ, we developed a binning protocol for each site as follows:

(1) Sort all 30-minute data points in order of increasing τ. For the first bin, set $\tau_{min,1}$ as the minimum of all the τ for the site.

(2) Add points to this bin in order of increasing τ until the bin is considered full by the following criterion:
    a. $\tau_{max,i} - \tau_{min,i} \geq 0.01$ Pa, AND
    b. There are at least 3 points in the bin OR $\tau_{max,i} - \tau_{min,i} > 0.025$ Pa.
(3) Once the current bin *i* is full, create a new bin i+1 with $\tau_{min,i+1}$ equal to the next value of τ from the ordered list. Then repeat steps 2 and 3 until all values have been assigned to bins.

Condition 2a was created to ensure that each bin covers a reasonably wide range of τ (comparable to typical random errors in τ), while condition 2b was created to balance the priorities of including sufficient data points in bins without creating excessively wide bins. Although our selection of binning criteria was necessarily arbitrary, we found that reasonable changes in our binning protocol would not have qualitatively affected any of our conclusions.

Estimation of binned values and their uncertainties

Let a_j and σ_{a_j} denote individual unbinned 30-minute values and their uncertainties for variable a within a certain τ bin *i*. We computed each binned value a_i as an arithmetic average

$$a_i = \sum_j a_j / N_i \tag{S5}$$

where N_i is the number of values in the bin. We estimated the binned value uncertainty σ_{a_i} by two separate methods: (1) propagation of the random errors of the constituent data points, and (2) the standard error of the N_i values of a_j. We computed the uncertainty associated with random errors σ_{μ,a_i} *(equation 4.19 in 90)* as

$$\sigma_{\mu,a_i} = \sqrt{\frac{1}{\sum_j \left(1/\sigma_{a_j}^2\right)}} \tag{S6}$$

This calculation represents the uncertainty associated with measurement errors that we can quantify and that are discussed in *(83)*. We also computed the bin standard error σ_{SE,a_i}

$$\sigma_{SE,a_i} = \frac{\sqrt{\frac{1}{N_i}\sum_j (a_j - a_i)^2}}{\sqrt{N_i}} \tag{S7}$$

This calculation represents the systematic uncertainty associated with differences in measured values due to all sources of error, including those that we were not able to quantify, such as changes in soil conditions. We then estimated the overall uncertainty in a_i as

$$\sigma_{a_i} = \max(\sigma_{SE,a_i}, \sigma_{\mu,a_i}) \quad \text{(S8)}$$

Conservatively taking the bin uncertainty as the maximum of these two methods helped to ensure that a realistic error was assigned to each binned value, such as in cases where the bin contained few constituent values, or when unquantified systematic errors contributed a substantial fraction of the total uncertainty.

Although the above binning procedure was meant to provide sufficient values in each bin to compute a standard error, sometimes a bin contained insufficient values for computation of standard error due to condition 2b above. We denote these bins with insufficient values (those with fewer than 3 data points) as 'sparse' bins. We estimated 'modified' standard errors σ'_{SE,a_i} for sparse bins based on 'comparable' bins at the same site containing 3 or more data points. For each comparable bin i, we computed the standard deviation of the values in the bin SD_{a_i}, then we computed the median of these values $SD_{med,a}$ across all bins. The calculation for $SD_{med,a}$ is illustrated in fig. S6 for saltation flux Q. Based on the typical standard deviation for binned values, we then estimated modified standard errors for the sparse bins as

$$\sigma'_{SE,a_i} = \frac{SD_{med,a}}{\sqrt{N_i}} \quad \text{(S9)}$$

where N_i is the number of data points in the bin. For the sparse bins, values of σ'_{SE,a_i} were then used instead of σ_{SE,a_i} for calculation of σ_{a_i} in equation S8. For saltation flux, a few of the calculated modified standard errors σ'_{SE,Q_i} unrealistically exceeded the associated flux values Q_i. In these cases, we adjusted the values so that $\sigma'_{SE,Q_i} = Q_i$.

We applied the above binning procedure to 30-minute values of τ, u_*, z_q, and Q. This yielded binned values τ_i, $u_{*,i}$, $z_{q,i}$, and Q_i, with associated bin uncertainties σ_{τ_i}, $\sigma_{u_{*,i}}$, $\sigma_{z_{q,i}}$, and σ_{Q_i}. For computation of binned saltation layer heights $z_{q,i}$ and associated uncertainties $\sigma_{z_{q,i}}$, we included only those 30-minute values z_q with corresponding 30-minute total saltation fluxes that were

nonzero, i.e., $Q > 0$. We applied this restriction because z_q is undefined for $Q = 0$. The effect of the binning procedure can be seen by comparing fig. S4, which shows 30-minute values of z_q versus u_*, to Fig. 1A (main text), which shows binned z_q versus u_*.

Analysis of literature data

In this section, we describe analysis of the three literature data sets for saltation layer heights: Greeley et al. (1996) *(57)*, Namikas (2003) *(58)*, and Farrell et al. (2012) *(59)*. In Fig. 1 of the main text, we compared saltation layer heights z_q computed from these literature data to the values of z_q calculated at our own field sites.

We note here that we considered two additional sets of field-based measurements of saltation flux profiles reported in the literature – Ellis et al. (2009) *(91)* and Dong et al. (2012) *(92)* – but we decided not to include these in our analysis. We excluded these datasets because the associated papers did not report values of shear velocity or shear stress to accompany the saltation flux profile data. In addition, although Dong et al. reported a trend of increasing z_q with wind strength, which contrasts with the main result of our paper, such trend probably is not statistically significant for their "open shifting sand plot" case that represents natural saltation over an erodible bed *(Fig. 7 in 92)*.

Greeley et al. (1996)

We obtained data from the flux profiles shown in Fig. 11 of Greeley et al. *(57)*. We estimated z_q and corresponding uncertainty σ_{z_q} for each saltation flux profile based on an exponential fit (equation 4 in main text). We obtained shear velocities u_* for corresponding runs directly from Table 1 in the main text. We chose $d_{50} = 0.23$ mm based on the "modal distribution" value stated in the paper. Although exact coordinates for the field site were not provided, the site described in the paper appears to be located close to our Oceano site.

Namikas (2003)

We obtained data from the flux profiles shown in Fig. 6 of Namikas *(58)*. We estimated z_q and corresponding uncertainty σ_{z_q} for each saltation flux profile based on an exponential fit (equation 4 in main text). We obtained shear velocities u_* for corresponding runs directly from Table 2 in the paper. We chose $d_{50} = 0.25$ mm based on the "averaged" value stated in the paper. Although exact coordinates for the field site were not provided, the site described in the paper appears to be close to our Oceano site.

Farrell et al. (2012)

We obtained shear velocities and flux profiles based on values listed in Table 1 of Farrell et al. *(59)*. For the analysis, we considered all runs at the "Cow Splat Flat Fine (CSFF)" site that included a value for u_*, except for Run 1, for which the trap duration was significantly shorter than for the other runs. Based on the site coordinates listed in the paper, CSFF was located within a few hundred meters of our Jericoacoara site. We ignored data from the "Cow Splat Flat Coarse (CSFC)" and "BEACH" sites listed in the paper, because these had different soil characteristics from CSFF but contained few data points. For each listed run at CSFF, we estimated the height-specific saltation flux q_i for each trap based on its collected mass, trap width, trap height, and duration, according to the same procedures described for our BSNE flux profile estimation *(equation 18 in 83)*. Table 1 in Farrell et al. provided only the bottom and top heights of the stacked traps, so we performed the exponential profile fitting to equation 4 (main text) iteratively to estimate trap heights z_i and saltation layer heights z_q. Since Farrell et al. did not report the particle size distribution at the surface, we could not include their data in the analysis of dimensionless saltation heights (Fig. 1C).

Data fitting and derivation of parameters

In this section, we describe methods for fitting to binned wind and saltation data to characterize saltation height versus shear velocity and total saltation flux versus shear stress trends. These fits correspond to the values listed in Table 1 and 2 of the main text.

Fitting saltation height versus shear velocity

In this subsection, we describe calculations of the mean saltation height and appraisal of its linear trend versus shear velocity. For calculations at our field sites, $z_{q,i}$ and $u_{*,i}$ refer to the individual binned values for each site. For the literature sites, $z_{q,i}$ and $u_{*,i}$ refer directly to the values from individual profile fits (i.e., no binning).

For each site, we performed a linear fit to saltation height $z_{q,i}$ versus shear velocity $u_{*,i}$, as

$$z_{q,fit,i} = a + bu_{*,i} \tag{S10}$$

where $z_{q,fit,i}$ are the predicted values for the linear fit. Intercept a, slope b, and associated uncertainties in these parameter fits (σ_a and σ_b) were calculated by the linear fitting procedure described in Section 5.1 of *(83)*. Values for b are shown in Fig. 1B (main text).

We calculated the mean saltation layer height for each site (Table 1 of main text) as

$$\langle z_q \rangle = \frac{\sum_i z_{q,i}}{N} \tag{S11}$$

where N is the number of bins for each site. The corresponding uncertainty in the mean saltation layer height was then calculated as the standard deviation

$$\sigma_{\langle z_q \rangle} = \sqrt{\frac{1}{N}\sum_i (z_{q,i} - \langle z_q \rangle)^2} \tag{S12}$$

We used the standard deviation rather than the standard error here because differences in individual $z_{q,i}$ reflected actual variability rather than measurement uncertainty.

The mean dimensionless saltation layer height is simply the ratio of the mean saltation layer height and the median surface particle diameter, $\langle z_q \rangle / d_{50}$. We applied error propagation (equation S3) to estimate associated uncertainty in dimensionless saltation layer height as

$$\sigma_{\langle z_q\rangle/d_{50}} = \frac{1}{d_{50}}\sqrt{\sigma^2_{\langle z_q\rangle} + \sigma^2_{d_{50}}\left(\langle z_q\rangle/d_{50}\right)^2} \quad \text{(S13)}$$

Fitting saltation flux versus shear stress

In this subsection, we describe our methods for performing fits to both the linear and the nonlinear 3/2 saltation flux law. These fits were applied to binned values of shear stress τ_i and total saltation flux Q_i at each site. Because the saltation flux law only applies when shear stress is above a threshold value τ_{it}, we removed certain low stress bins from the analysis for each site. However, since we lacked knowledge of τ_{it} prior to performing the fit, we required independent criteria for selecting the binned values to include in the fit. For this criterion, we chose a minimum transport frequency, below which saltation occurs very infrequently and equilibrium saltation transport conditions may never occur. In particular, we limited analysis to bins *i* for which saltation was detected for at least 10% of 1-second increments within the bin. The resulting binned values Q_i and τ_i for the fit, subject to the 10% limit, are shown in Fig. 2 (main text).

We evaluated the relative quality of linear and 3/2 fits by computing reduced chi-square χ^2_ν values, which express differences between best fit and the measured values, normalized by the number of degrees of freedom υ (number of data points minus number of fitting parameters, which is 2 for both linear and 3/2 fits)

$$\chi^2_\nu = \frac{1}{\upsilon}\sum_i \frac{\left(Q_i - Q_{fit,i}\right)^2}{\sigma^2_{Q_i total}} \quad \text{(S15)}$$

where Q_i are the observed (bin-averaged) total saltation fluxes and $Q_{fit,i}$ are the expected saltation fluxes for linear or 3/2 fits. $\sigma_{Q_i,total}$ are total uncertainties in observed saltation fluxes, computed as

$$\sigma_{Q_{i,total}} = \sqrt{\sigma_{Q_i}^2 + \sigma_{Q,\tau_i}^2} \tag{S16}$$

σ_{Q_i} are uncertainties for binned saltation fluxes and σ_{Q,τ_i} are additional contributions of shear stress uncertainty σ_{τ_i} to total saltation flux uncertainty. For the linear fit, we applied error propagation (equation S3) to equation 12 (main text) to get

$$\sigma_{Q,\tau_i} = C\sigma_{\tau_i} \tag{S17}$$

For the 3/2 fit, we applied error propagation to equation 13 (main text) to get

$$\sigma_{Q,\tau_i} = \sigma_{u_{*,i}} C|3\tau_i - \tau_{it}| \tag{S18}$$

To obtain fit parameters, C and τ_{it}, and expected saltation fluxes $Q_{fit,i}$, we performed fits to linear and 3/2 versions of the flux law (equations 12 and 13 and Fig. 2 in main text). For the linear flux law, we applied the linear fitting procedure described in *(83)*. For the 3/2 nonlinear flux law fit, we applied an iterative procedure to determine the values of C and τ_{it} that minimize χ_ν^2, and we obtained uncertainties in fitting parameters (σ_C and $\sigma_{\tau_{it}}$) from the ranges of C and τ_{it} for which $\chi^2 \leq \min(\chi^2) + 1$, where χ^2 is the non-reduced chi-square value, i.e., $\chi_\nu^2 = \frac{\chi^2}{\upsilon}$.

The resulting linear and 3/2 fits are shown in Fig. 2 (main text) and associated fit parameters, C and τ_{it}, are listed in Table 2 (main text). χ_ν^2 describes the extent to which the fitted function explains the measured data and its uncertainty. A value of $\chi_\nu^2 \approx 1$ indicates that the model reasonably describes the observational data within the uncertainties, whereas a value of $\chi_\nu^2 \gg 1$ indicates either that the model does not capture all of the variance of the data, or that the uncertainty in the measurements is underestimated *(90)*. At Jericoacoara and Oceano, the values

for χ_v^2 were substantially smaller for the linear fit than for the nonlinear 3/2 fit, indicating the superiority of the linear flux law. At Rancho Guadalupe, χ_v^2 values were similar for linear and nonlinear 3/2 fits, indicating that neither fit was preferable. At Jericoacoara and Oceano, $\chi_v^2 > 1$ indicates some underestimation of the saltation flux uncertainties. At Rancho Guadalupe, $\chi_v^2 < 1$ indicates some overestimation of the saltation flux uncertainties. These differences might indicate that data at these sites were insufficient to fully characterize the variability in saltation flux.

Calculation of excess stress

We calculated the excess stress as

$$\tau_{ex,i} = \tau_i - \tau_{it} \tag{S19}$$

where τ_i is the binned shear stress and τ_{it} is the impact threshold from the linear fit (equation 12 and Table 2 in main text). The uncertainty in excess stress $\sigma_{\tau_{ex,i}}$ depended both on uncertainty in binned values of shear stress σ_{τ_i} and uncertainty in the threshold stress $\sigma_{\tau_{it}}$ through error propagation (equation S3)

$$\sigma_{\tau_{ex,i}} = \sqrt{\sigma_{\tau_i}^2 + \sigma_{\tau_{it}}^2} \tag{S20}$$

Based on the linear best fit threshold shear stress τ_{it}, we estimated the associated shear velocity threshold as $u_{*it} = \sqrt{\tau_{it}/\rho_f}$. We then calculated the corresponding uncertainty in shear velocity threshold by error propagation (equation S3)

$$\sigma_{u_{*it}} = \frac{\sigma_{\tau_{it}}}{2\sqrt{\rho_f \tau_{it}}} \tag{S21}$$

The values of shear velocity threshold and their associated uncertainties are listed in Table 1 (main text).

Calculation of normalized saltation flux

We calculated normalized saltation flux $\hat{Q}_i$ for stress bin *i* by equation 14 (main text). We estimated corresponding uncertainty in $\hat{Q}_i$ through error propagation (equation S3)

$$\sigma_{\hat{Q},i} = \hat{Q}_i \sqrt{\left(\frac{\sigma_{Q_i}}{Q_i}\right)^2 + \left(\frac{\sigma_{u*,it}}{u_{*,it}}\right)^2} \quad \text{(S22)}$$

Parameterization of flux law

We estimated the flux law parameterization C_Q for each site by rearranging equation 15 (main text) and computing the average

$$C_Q = \langle \frac{\hat{Q}_i}{\tau_{ex,i}} \rangle \quad \text{(S23)}$$

where the brackets refer to the average over all $\frac{\hat{Q}_i}{\tau_{ex,i}}$ ratios. To prevent widely variable near-threshold values from heavily skewing the calculation of C_Q (and the calculation of C_t below), we included only those bins *i* for which all of the individual τ_{ex} in the bin exceeded $2\sigma_{\tau_{it}}$, i.e., outside the 95% confidence range for τ_{it}. We estimated the corresponding uncertainty in C_Q as the mean-squared difference between the mean and individual values of this ratio

$$\sigma_{C_Q} = \sqrt{\frac{1}{N}\sum_i \left(\frac{\hat{Q}_i}{\tau_{ex,i}} - \langle \frac{\hat{Q}_i}{\tau_{ex,i}} \rangle\right)^2} \quad \text{(S24)}$$

where N is the number of bins included in the calculations for each site. The resulting values of C_Q and σ_{C_Q} are given in Table 1 (main text). To estimate the combined average value of C_Q and its uncertainty across all sites, we applied equations S5 and S6 to the values of C_Q and σ_{C_Q} from the three sites.

An alternative version of the flux law parameter is C_t (equation 9 in main text), which is given by

$$C_t = \frac{1-e}{\sqrt{\langle z_q \rangle / g}} \langle \frac{Q_i}{\tau_{ex,i}} \rangle \quad \text{(S25)}$$

Because the restitution coefficient e is unknown, we instead calculated

$$\frac{C_t}{1-e} = \sqrt{\frac{g}{\langle z_q \rangle}} \langle \frac{Q_i}{\tau_{ex,i}} \rangle \quad \text{(S26)}$$

We then estimated uncertainty in $\frac{C_t}{1-e}$ as the mean-squared difference between the mean and individual values of this ratio

$$\frac{\sigma_{C_t}}{1-e} = \sqrt{\frac{1}{N}\frac{g}{\langle z_q \rangle}\sum_i \left(\frac{Q_i}{\tau_{ex,i}} - \langle\frac{Q_i}{\tau_{ex,i}}\rangle\right)^2} \quad \text{(S27)}$$

The resulting values for parameter $C_t/(1-e)$ and their uncertainties were 2.5 ± 0.3 for Jericoacoara, 1.7 ± 0.1 for Rancho Guadalupe, and 2.2 ± 0.4 for Oceano.

List of variables

Below, we list all variables described in the main text and supplementary text. Typical units for variables are given in brackets.

Variables in main text (in order of appearance)

Q, vertically-integrated saltation mass flux [g $m^{-1}s^{-1}$]

τ, wind shear stress [Pa = kg $m^{-1}s^{-2}$]

Φ, vertically-integrated saltation layer mass concentration [kg m^{-2}]

V, mean horizontal particle speed [m s^{-1}]

τ_{it}, impact threshold shear stress [Pa]

τ_{ex}, excess shear stress [Pa]

u_*, wind shear velocity [m s^{-1}]

ρ_f, air density [kg m^{-3}]

z_q, saltation layer (e-folding) height [m]

$q(z)$, vertical profile of saltation flux, [gm^{-2}]

z, height above the sand bed [m]

q_0, saltation profile scaling parameter [g $m^{-2}s^{-1}$]

$\langle z_q \rangle$, mean saltation layer height for site [m]

d_{50}, median diameter of surface particles (by volume) for site [mm]

τ_p, particle momentum dissipation rate [Pa]

M, mass collision rate per unit bed area [kg $m^{-2}s^{-1}$]

e, bulk restitution coefficient

t_{hop}, typical hop time for saltating particles [s]

z_{hop}, typical maximum hop height for saltating particles [m]

g, gravitational acceleration [m s^{-2}]

C_z, dimensionless constant relating z_{hop} and z_q (equation 8)

C_t, empirical scaling parameter for flux law (equation 9)

C_Q, empirical scaling parameter for flux law (equation 10)

$u_{*,it}$, impact threshold wind shear velocity [m s^{-1}]

Q_{linear}, total saltation flux for linear flux law fit [g $m^{-1}s^{-1}$]

$Q_{3/2}$, total saltation flux for 3/2 flux law fit [g $m^{-1}s^{-1}$]

C, fitting parameter for linear flux law fit [s] or 3/2 flux law fit [$m^{-1}s^2$]

χ_v^2, normalized mean-squared difference between observations and predictions

$\hat{Q}$, normalized saltation flux (equation 14) [Pa]

s, particle-fluid density ratio

ρ_p, particle density [kg m^{-3}]

z/L, stability parameter

u, streamwise wind velocity [m s^{-1}]

u', fluctuating component of streamwise wind [m s^{-1}]

$\bar{u}$, mean streamwise wind velocity [m s^{-1}]

w, vertical wind velocity [m s^{-1}]

w', fluctuating component of vertical wind [m s^{-1}]

$\bar{w}$, mean vertical wind velocity [m s^{-1}]

b, slope parameter for fit of z_q versus u_*

Variables in supplementary text (in order of appearance)

θ, wind angle

$\langle\theta\rangle$, site-averaged wind angle during saltation

v, spanwise wind velocity [m s^{-1}]

$\bar{v}$, mean spanwise wind velocity [m s^{-1}]

σ_τ, shear stress uncertainty [Pa]

σ_{u_*}, shear velocity uncertainty [m s^{-1}]

y, variable for uncertainty propagation

σ_y, uncertainty in variable for uncertainty propagation

$x_1, x_2, \ldots$, quantities affecting y uncertainty

$\sigma_{x_1}, \sigma_{x_2}, \ldots$, uncertainties in $x_1, x_2, \ldots$

T, air temperature [K]

T', fluctuating component of air temperature [K]

$\bar{T}$, mean air temperature [K]

κ, von Karman parameter ($\approx$0.4)

z_U, anemometer height [m]

$\tau_{min,i}$, minimum wind shear stress for stress bin i [Pa]

$\tau_{max,i}$, maximum wind shear stress for stress bin i [Pa]

a_j, individual unbinned 30-minute values for generic variable a

σ_{a_j}, uncertainties for individual unbinned 30-minute values for generic variable a

a_i, binned value of generic variable a for stress bin i

σ_{a_i}, uncertainty for binned value of generic variable a for stress bin i

N_i, number of values in stress bin i

σ_{μ,a_i}, uncertainty for binned value of generic variable a associated with measurement errors

σ_{SE,a_i}, uncertainty for binned value of generic variable a associated with bin standard error

σ'_{SE,a_i}, modified bin standard error uncertainty for binned value of generic variable a

SD_{a_i}, standard deviation for generic variable a for stress bin i

$SD_{med,a}$, median standard deviation for binned variable a for bins containing at least 3 values

SD_{Q_i}, standard deviation for binned saltation flux Q_i values [g m^{-1}s^{-1}]

σ'_{SE,Q_i}, modified standard error in total saltation flux for stress bin i [g m^{-1}s^{-1}]

σ_{z_q}, uncertainty in characteristic e-folding saltation layer height [m]

$z_{q,fit,i}$, predicted value for linear best fit of $z_{q,i}$ versus $u_{*,i}$

σ_b, uncertainty in slope for fit of z_q versus u_* [s]

N, total number of stress bins

$\sigma_{\langle z_q \rangle}$, uncertainty in mean saltation layer height [m]

$\sigma_{\langle z_q \rangle / d_{50}}$, uncertainty in mean dimensionless saltation layer height for site

$\boldsymbol{\upsilon}$, degrees of freedom for fit

χ^2, mean-squared difference between observations and predictions

$Q_{fit,i}$, predicted value for fit of saltation flux versus shear stress for stress bin i [g m^{-1}s^{-1}]

$\sigma_{Q_i,total}$, total saltation flux uncertainty (including propagated stress uncertainty) [g m^{-1}s^{-1}]

σ_{Q,τ_i}, uncertainty in saltation flux for stress bin i due to uncertainty in shear stress [g m^{-1}s^{-1}]

σ_C, uncertainty in generic fitting parameter for linear flux law fit [s] or 3/2 flux law fit [m^{-1}s^2]

$\sigma_{\tau_{it}}$, uncertainty in impact threshold shear stress [Pa]

$\sigma_{\tau_{ex}}$, excess stress uncertainty [Pa]

$\sigma_{u_{*,it}}$, uncertainty in impact threshold shear velocity [m s^{-1}]

$\sigma_{\hat{Q},i}$, uncertainty in normalized saltation flux [Pa]

σ_{C_Q}, uncertainty in fitting parameter for linear stress-flux relationship

σ_{C_t}, uncertainty in alternative fitting parameter for linear stress-flux relationship

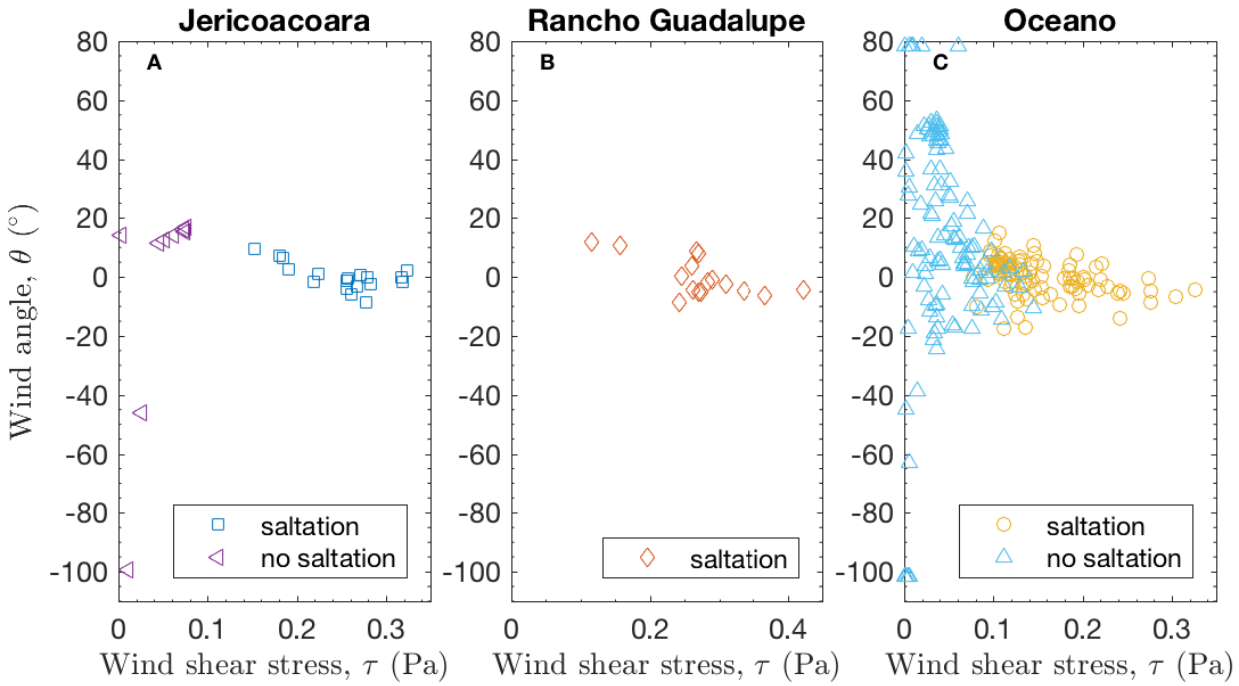

fig. S1. Wind angle θ versus shear stress τ over individual 30-min intervals at the three field sites. All measurements at Rancho Guadalupe were made during saltation. Periods of detected saltation transport and no transport are distinguished by different symbols at Jericoacoara and Oceano.

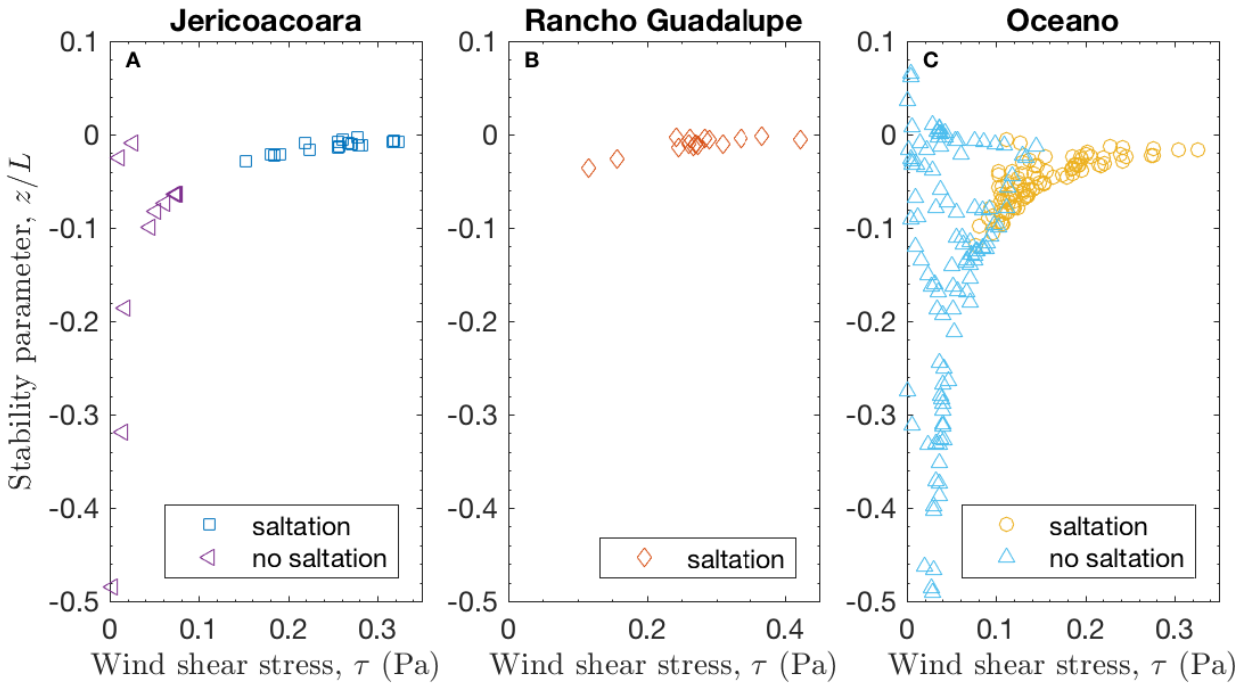

fig. S2. Stability parameter $\frac{z}{L}$ versus shear stress τ over individual 30-min intervals at the three field sites. Periods of detected saltation and no saltation are distinguished by different symbols at Jericoacoara and Oceano. Some extreme values for $\frac{z}{L}$ are outside of the range of the plots, but these correspond only to intervals with no saltation.

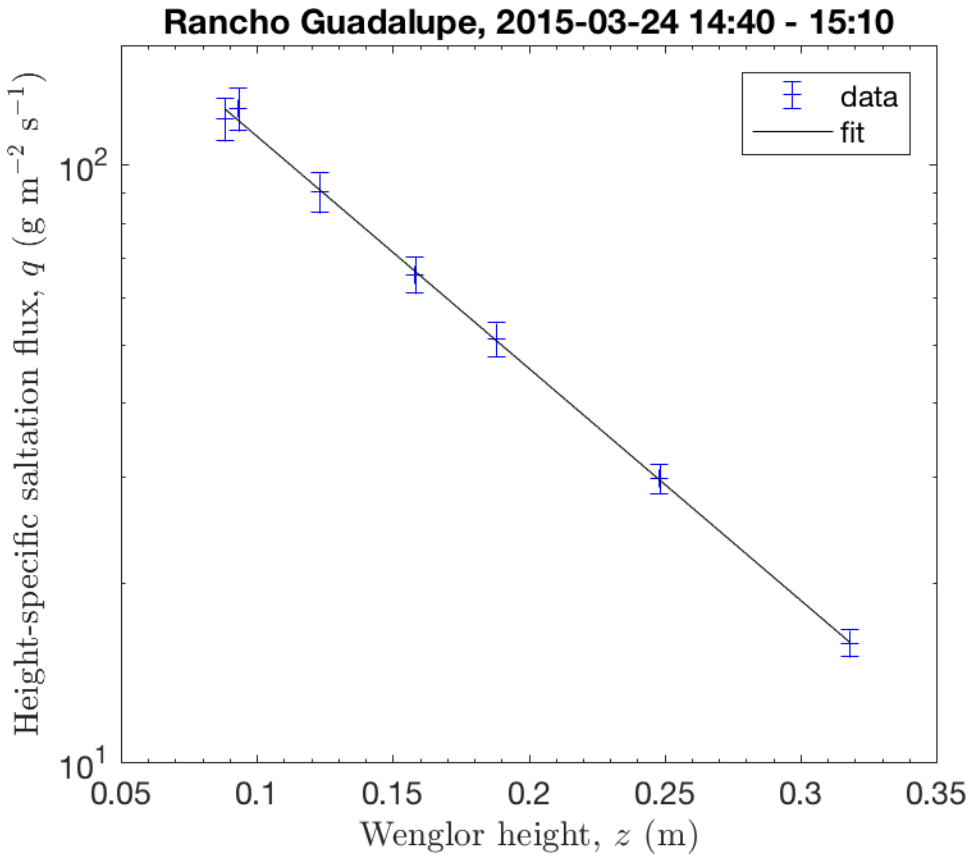

fig. S3. Typical 30-min vertical profile of saltation flux. Crosses indicate calibrated Wenglor height-specific horizontal saltation fluxes q versus heights z. Vertical bars indicate uncertainties in q. Solid line is fit to exponential profile (equation 4 in main text).

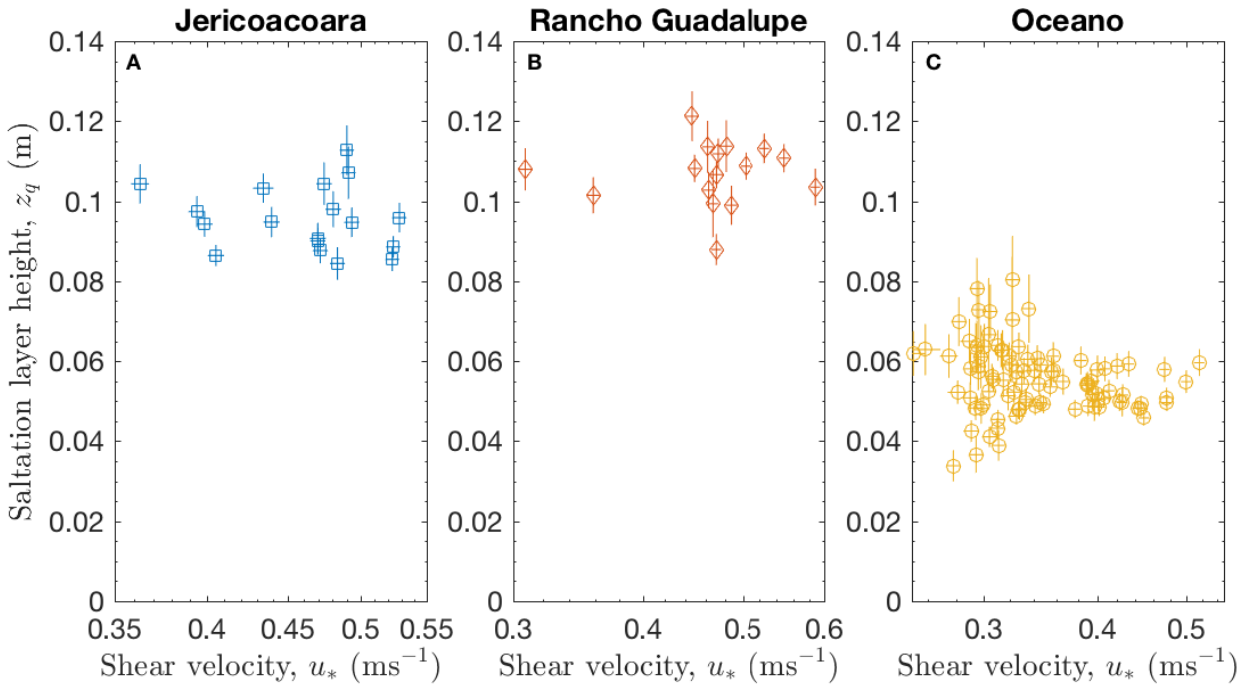

fig. S4. Thirty-minute values of saltation layer height z_q versus shear velocity u_* at the three field sites. Vertical error bars indicate saltation layer height uncertainties σ_{z_q}; horizontal error bars, shear velocity uncertainties σ_{u_*}. Only those 30-minute time increments for which saltation was active are plotted here.

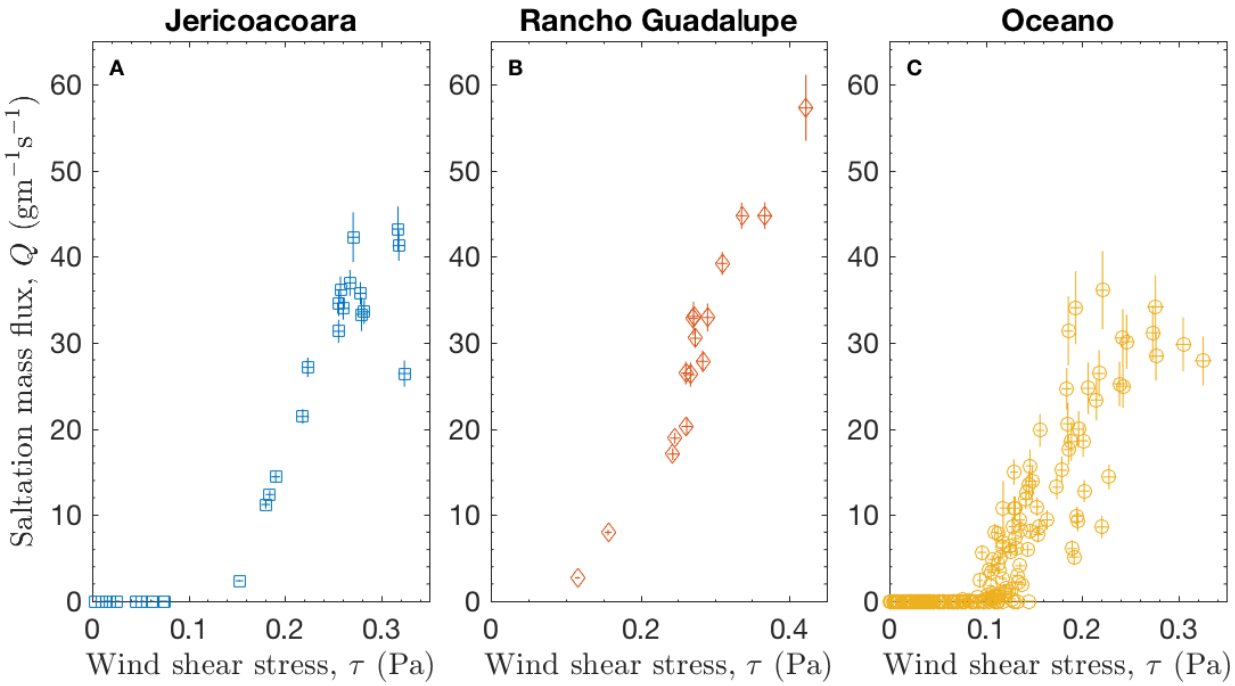

fig. S5. Thirty-minute values of saltation mass flux *Q* versus wind shear stress τ at the three field sites. Measurements at (**a**) Jericoacoara, (**b**) Rancho Guadalupe, and (**c**) Oceano. Vertical error bars indicate flux uncertainties σ_Q; horizontal error bars, stress uncertainties σ_τ.

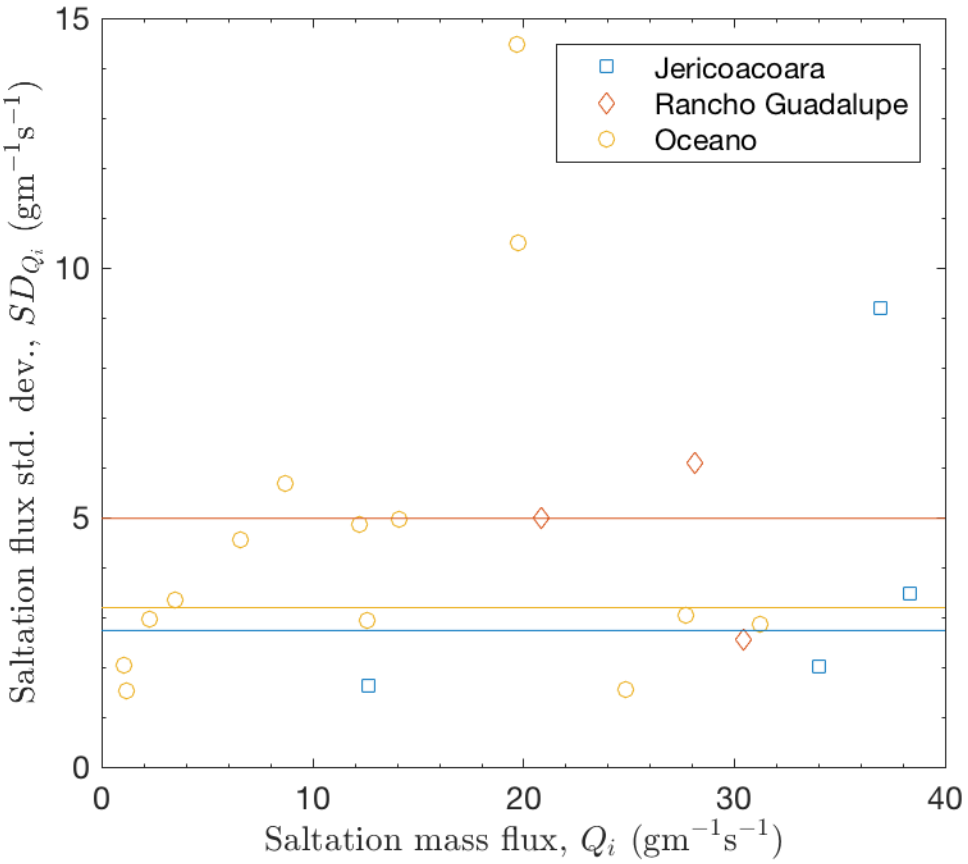

fig. S6. SD of saltation flux values within individual stress bins *i*, SD_{Qi}, versus bin-averaged saltation fluxes, Q_i. Only those bins containing at least 3 values are plotted. Solid lines show resulting median values of standard deviations $SD_{med,Q}$ for each site. These $SD_{med,Q}$ were then used to calculate standard errors for sparse bins containing fewer than three data points.

data file S1. Excel spreadsheet (.xlsx) containing unbinned 30-min values for shear velocity u_*, shear stress τ, wind direction θ, stability parameter z/L, saltation layer height z_q, total saltation flux Q, saltation detection frequency f_Q, and associated uncertainties for all of these values (except θ, z/L, and f_Q) for each field site. Data may also be accessed through the Zenodo data repository at http://doi.org/10.5281/zenodo.291798.

data file S2. Excel spreadsheet (.xlsx) containing binned 30-min values for shear velocity u_*, shear stress τ, excess shear stress τ_{ex}, saltation layer height z_q, total saltation flux Q, normalized saltation flux $\hat{Q}$, saltation detection frequency f_Q, and associated uncertainties for all of these values. The spreadsheet also lists the numbers of 30-minute values in each bin for each field site. Data may also be accessed through the Zenodo data repository at http://doi.org/10.5281/zenodo.291799.